Effects of Gas Flow Field on Clogging Phenomenon in Close-Coupled Vortical Loop Slit Gas Atomization

ZHANG Min[1], *ZHANG Zhaoming*[1*], *ZHANG Yanqi*[1], *LU Yuanjing*[1], *LU Lin*[2]

1. College of Aerospace Engineering, Nanjing University of Aeronautics and Astronautics, Nanjing 210016, P. R. China;
2. Shanghai Research Institute of Materials, Shanghai 200437, P. R. China

(Received 15 January 2021; revised 17 September 2021; accepted 10 October 2021)

Abstract: In order to study the basic characteristics of gas flow field in the atomizing chamber near the nozzle outlet of the vortical loop slit atomizer and its influence mechanism on clogging phenomenon, the computational fluid dynamics (CFD) software Fluent is used to conduct a numerical simulation of the gas flow field in the atomizing chamber near the nozzle outlet of this atomizer under different annular slit widths, different atomization gas pressures and different protrusion lengths of the melt delivery tube. The results show that under atomization gas pressure $p = 4.5$ MPa, the greater the annular slit width D, the lower the static temperature near the central hole outlet at the front end of the melt delivery tube, and the smaller the aspirating pressure at the front end of the melt delivery tube. These features can effectively prevent the occurrence of the clogging phenomenon of metallic melt. Under an annular slit width of $D = 1.2$ mm, when the atomization gas pressure satisfies 1 MPa $\leqslant p \leqslant$ 2 MPa and increases gradually, the aspirating pressure at the front end of the melt delivery tube will decline rapidly. This can prevent the clogging phenomenon of metallic melt. However, when the atomization gas pressure $p >$2 MPa, the greater the atomization gas pressure, the lower the static temperature near the central hole outlet at the front end of the melt delivery tube, and the greater the aspirating pressure at the front end of the melt delivery tube. Hence, the effect of preventing the solidification-induced clogging phenomenon of metallic melt is restricted. When atomization gas pressure is $p =$ 4.5 MPa and annular slit width is $D = 1.2$ mm, the greater the protrusion length H of the melt delivery tube, and the smaller the aspirating pressure at its front end. The static temperature near the central hole that can be observed in its front end is approximate to effectively prevent the occurrence of clogging phenomenon of metallic melt. However, because of the small aspirating pressure, the metallic melt flows into the atomizing chamber from the central hole at the front end of the melt delivery tube at an increasing speed and the gas-melt ratio in the mass flow rate is reduced, which is not conducive to the improvement of atomization performance.

Key words: vortical loop slit atomizer; annular slit width; atomization gas pressure; melt delivery tube protrusion length; gas flow field; numerical simulation

CLC number: TF123.2 **Document code:** A **Article ID:** 1005-1120(2021)06-1003-17

0 Introduction

Airflow atomization is the main method that uses the atomizing medium to crush liquid metal or alloy directly to prepare powders and high-performing rapidly solidifying materials. The atomizer is an atomizing device that enables the atomizing medium to achieve high energy and high speed and to pulverize the metal solution. It plays an important role in atomizing efficiency and stability of the atomizing process. The prepared metal powders have advantages, such as a high degree of sphericity, controllable powder size, low oxygen content, and high applicability to the production of all kinds of metal and alloy powders. This process has become the main method for producing high-performance metal and

*Corresponding author, E-mail address: zzm603nuaa@163.com.

How to cite this article: ZHANG Min, ZHANG Zhaoming, ZHANG Yanqi, et al. Effects of gas flow field on clogging phenomenon in close-coupled vortical loop slit gas atomization[J]. Transactions of Nanjing University of Aeronautics and Astronautics, 2021, 38(6): 1003-1019.

http://dx.doi.org/10.16356/j.1005-1120.2021.06.011

special alloy powders[1]. The two types of commonly used atomizers are the 2-D axisymmetric loop slit (or loophole) atomizer and the vortical loop slit atomizer. The loop slit atomizer has advantages of simple structure and easy machining over ring-hole atomizer and the loop slit can be made into contraction-type or Laval-shaped nozzle. This shape indicates that airflow outlet velocity is approximate to or exceeds sound velocity to break up metal melt effectively into smaller liquid drops with a high yield of fine powders. This type of atomizer is used commonly in airflow atomization methods. However, the loop slit atomizer is very sensitive to the structural parameters of the nozzle and operating parameters. A light change will result in obvious differences in the atomizing effect of the atomizer and can more seriously lead to clogging phenomenon such that powder production by atomization becomes impossible[2-3]. Over the years, considerable attention has been given to the exploration of the powder production process. Anderson et al.[4] investigated the change rules of aspirating pressure at the front end of the melt delivery tube with atomization gas pressure for different end shapes of ultra-sonic gas atomization (USGA) atomizing nozzles. Mi et al.[5-6] used computational fluid dynamics (CFD) software Phoenics to simulate the effects of atomization gas pressure and structural parameters of the nozzle in the loop slit high pressure gas atomization (HPGA) nozzle on the gas flow field. Cui et al.[7] conducted a comparative study of the formation mechanisms in the front-end pressure intensity zone of the melt delivery tube in the atomizing process of Laval-and contraction-type atomizing nozzles and believed that Laval-type nozzle had higher atomizing efficiency than the contraction-type nozzle. Mates et al.[8] studied the effect of atomization gas pressure in the close-coupled atomizing nozzle on the gas flow field and believed that the convergent-divergent nozzle did not produce finer powder than the convergent nozzle at stagnation pressures where they produced similarly long gas-only supersonic jets and conducted an experimental verification. Zeoli et al.[9] used Fluent software to study the breakup, cooling, and solidification phenomenon of metal melt in the atomizing process through the loop slit isentropic plug nozzle (IPN) nozzle and pointed out that droplets have very similar profiles during gas atomization and the major factor influencing the atomization and solidification process of droplets are in-flight distance. Li et al.[10] implemented a detailed study of the breakup, cooling, and solidification coupling process of metal melt in the vortical atomizer and provided a research direction for exploring primary and secondary breakup processes of metal melt in the vortical atomizer, and propose the characteristics of liquid slice breakage. Based on a study of the working mechanism of the vortical loop slit atomizer, Chen et al.[11] pointed out that fluid atomizing medium would not focus on a point after being ejected from the vortical loop slit atomizer, but instead, would form a hollow double cone body. To avoid choking, the protrusion length of the melt delivery tube should be such that the upper negative pressure zone of the bottle opening of the hollow double cone is closed in theory. Liu[12] conducted an analytical investigation of the design parameters of the vortical loop slit atomizer and proposed a qualitative explanation and quantitative description of design parameters. Ma et al.[13] used Fluent to conduct a numerical simulation of the gas flow field inside the vortical loop slit atomizer and at the nozzle outlet. Motaman et al.[14] studied the effect of the gas flow angle of the nozzle on backflow at the outer wall surface along the protrusion length of the melt delivery tube in the close-coupled gas atomization process, in the investigation a Convergent-Divergent (C-D) discrete gas jet die at five different atomization gas pressures of 1—5 MPa, with different gas exit jet distances of 1.65, 1.6, 1.55, 1.5, 1.45 and 1.40 mm from the melt nozzle external wall, was combined with four melt nozzles of varying gas jet mis-match angles of 0°, 3°, 5°, and 7° relative to the melt nozzle external wall. Aydin et al.[15] used Fluent to study the effects of pressure intensity at the inlet of the close-coupled atomizing nozzle on the aspirating pressure at the front end of the melt delivery tube and flow separation on the outer wall surface of the protrusion length and carried out an experimental verification, atomization gas pressures of 1.0, 1.3, 1.7, 2.2, and 2.7 MPa were used in the CFD model to initialize the pressure in gas inlet. Prashan-

th et al.[16] studied the effect of the melt delivery tube (MDT) position on atomization outcomes such as the yield, mass median diameter, and spread of the particle size distribution. Zhang et al.[17] used Fluent to conduct a numerical simulation study on the gas flow field characteristics of the vortical loop slit atomizer. Maly et al.[18] used phase Doppler anemometry (PDA) and high-speed imaging to conduct design and experimental research on the small spill-return atomizers (SRAs). Fan et al.[19] used high-speed shadowgraph technique to study the spray characteristics of a pressure-swirl atomizer under different pressure drops and fuel temperatures. Ochowiak.[20] presented the experimental research results of the atomization process of the effervescent atomizers with the swirl motion flow, and analyzed in detail the influence of the shape of the atomizer on the pressure drops and the discharge coefficient was performed. Razeghi et al.[21] studied the fluid flow details and characteristics inside a pulse-mode operating pressure swirl atomizer (PSA). Wang et al.[22] studied the influence mechanism of gas temperatures (300, 400, 500, and 600 K) on gas atomization by simulating the integral atomization process of the close-coupled nozzle in vacuum induction gas atomization (VIGA). Despite numerous studies, research on the influencing mechanism of the clogging phenomenon of vortical loop slit atomizer with structural parameters of the nozzle and operating parameters remains lacking.

The atomizing process of gas flow is associated with the actual atomizing process. The close-coupled supersonic vortical loop slit atomizer was used by the Shanghai Research Institute of Materials in the actual production process. A numerical simulation method is adopted to investigate the influencing mechanism of annular slit width, atomization gas pressure, and protrusion length of melt delivery tube on basic features of the gas flow field in the atomizing chamber near the atomizing nozzle outlet. A clogging phenomenon near the central hole outlet at the front end of the melt delivery tube because the solidification of metal melt is investigated. The research is expected to provide a basis for high-efficiency atomizing nozzle design and operation and recognition of the atomizing phenomenon.

1 Description of Physical Model

The study object is a close-coupled supersonic vortical loop slit gas atomization nozzle, as shown in Fig.1, where α is the cone-apex angle of melt delivery tube of metal melt, β the gas flow angle of the nozzle, $\alpha = \beta = 60°$, H the protrusion length of melt delivery tube, and D the annular slit width. The gas chamber of the nozzle is connected to the inlet pipe and high-pressure gas source. The pressure of the inlet pipe is controlled by a regulating valve and atomization gas is nitrogen.

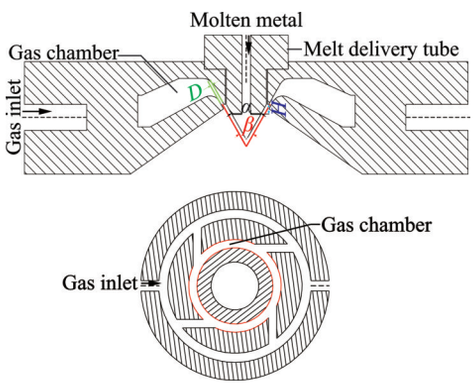

Fig.1 Structural diagram of atomizer and melt delivery tube

For the convenience of constructing a flow model of atomization gas, the following hypotheses are proposed: (1) Gas flow in the nozzle is steady flow; (2) atomization gas flow is isentropic compressive flow and follows ideal gas law $p_s = \rho RT$, where p_s is the static pressure, ρ the density, R the ideal gas constant, and T the static temperature; (3) both mass transfer and momentum transfer exist between gas flow layers; (4) the effect of gravity on gas flow is neglected.

2 Mathematical Model and Computing Method

2.1 Fluid dynamics control equation

The continuity equation is

$$\frac{\partial \rho}{\partial t} + \frac{\partial}{\partial x_i}(\rho u_i) = 0 \tag{1}$$

The momentum equation (Navier-Stokes equation) is

$$\frac{\partial}{\partial t}(\rho u_i)+\frac{\partial}{\partial x_j}(\rho u_i u_j)=-\frac{\partial p_s}{\partial x_i}+\frac{\partial}{\partial x_j}\left[\mu\left(\frac{\partial u_i}{\partial x_j}+\frac{\partial u_j}{\partial x_i}\right)-\frac{2}{3}\mu\frac{\partial u_l}{\partial x_l}\delta_{ij}\right] \tag{2}$$

where ρ is the density; u_i the velocity component in the x_i-direction ($i=1, 2, 3$ or x, y, z); u_j the velocity component in the x_j-direction ($j=1, 2, 3$ or x, y, z); u_l the velocity component in the x_l-direction ($l=1, 2, 3$ or x, y, z); μ the dynamic viscosity coefficient; and δ_{ij} the Kronecker delta.

The energy equation is

$$\frac{\partial}{\partial t}(\rho T)+\frac{\partial}{\partial x_j}(\rho u_j T)=\frac{\partial}{\partial x_j}\left[\frac{K}{c_V}\frac{\partial T}{\partial x_j}-\frac{2}{5}\rho u_j T\right] \tag{3}$$

where K is the effective thermal conductivity coefficient of gas; T the static temperature; and c_V the specific heat capacity of gas.

The k-ω SST model[23] proposed by Menter has been used extensively in the numerical simulation of complex flow-like adverse-pressure gradient flow and shock wave (Because of the strong shock wave in the atomization flow field of the close-coupled vortical loop slit atomizer). In the SST-format k-ω model, the standard k-ω model is adopted in the boundary layer near the wall surface. The k-ε model is adopted at the edge of the boundary layer and at the free shear layer and is transited through a hybrid function and written uniformly into k-ω forms through coefficient superposition. In the expression of this model equation, equations of turbulence kinetic energy k and specific turbulence dissipation rate ω and hybrid function F_1 are as follows

$$\frac{\partial}{\partial t}(\rho k)+\frac{\partial}{\partial x_i}(\rho k u_i)=\frac{\partial}{\partial x_j}\left(\Gamma_k\frac{\partial k}{\partial x_j}\right)+G_k-Y_k+S_k \tag{4}$$

$$\frac{\partial}{\partial t}(\rho\omega)+\frac{\partial}{\partial x_i}(\rho\omega u_i)=\frac{\partial}{\partial x_j}\left(\Gamma_\omega\frac{\partial\omega}{\partial x_j}\right)+G_\omega-Y_\omega+D_\omega+S_\omega \tag{5}$$

$$F_1=\tanh(\Phi_1^4) \tag{6}$$

$$\Phi_1=\min\left[\max\left(\frac{\sqrt{k}}{0.09\omega y},\frac{500\mu}{\rho y^2\omega}\right),\frac{4\rho k}{\sigma_{\omega,2}D_\omega^+ y^2}\right] \tag{7}$$

$$D_\omega^+=\max\left(2\rho\frac{1}{\sigma_{\omega,2}}\frac{1}{\omega}\frac{\partial k}{\partial x_j}\frac{\partial\omega}{\partial x_j},10^{-20}\right) \tag{8}$$

where G_k is the generation term of turbulence kinetic energy k caused by average velocity gradient; G_ω the generated by the equation of the specific turbulence dissipation rate ω; D_ω the transverse dissipation derivative term; y the distance to the next surface; and D_ω^+ the positive portion of the cross-diffusion term. Γ_k and Γ_ω represent the effective diffusivity terms of k and ω, respectively; Y_k and Y_ω the dissipation terms of k and ω, respectively; and S_k and S_ω the user-defined source terms. The computing formulas of the terms in the equation and values of its sealed constants are obtained from Ref.[23].

2.2 Mesh generation

The preprocessing software Pointwise (ICEM CFD) 17.0 is used for modeling the flow field zone of the nozzle. During the modeling process, gas flow fields are placed vertically and high-pressure gas flows from the pressure inlet. Tetrahedral elements are generated in the meshing process, and when atomization gas leaves the nozzle, strong pressure and velocity gradient will appear, and thus, the meshes should be refined, and the minimum grid size is 0.3 mm. The gas flow located far from the nozzle outlet is steady, such that meshes are sparse, and the maximum grid size is 4 mm, as shown in Fig.2.

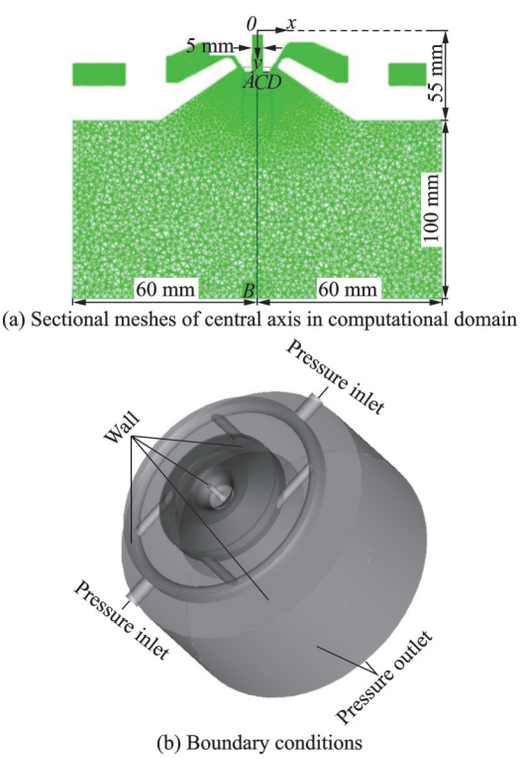

(a) Sectional meshes of central axis in computational domain

(b) Boundary conditions

Fig.2 Sectional meshes of central axis and boundary conditions in computational domain

2.3 Boundary conditions

The boundary conditions of the computational domain are shown in Fig.2, where the inlet boundary of the nozzle is set as the inlet boundary type of pressure intensity, the outlet boundary is set as outlet boundary type of pressure intensity, and others (including melt delivery tube) are set as wall-surface types. The boundary conditions are set as follows: the total temperature at nozzle inlet is 300 K, the outlet pressure intensity p_o is 96 700 Pa, and the temperature is 300 K. At the boundary of the wall surface is the near-wall flow, which is calculated through a standard wall-surface function. Atomization gas is nitrogen, which is processed according to an ideal gas. Its specific parameters are listed in Table 1. Gas viscosity is calculated by using the Sutherland formula

$$\mu = \mu_0 \left(\frac{T}{T_0}\right)^{\frac{3}{2}} \frac{T_0 + S}{T + S} \tag{6}$$

where μ is the viscosity, μ_0 the reference viscosity, T_0 the reference temperature, and S the effective temperature (also called Sutherland constant). Other parameters follow the default setting of Fluent 6.3 software. The specific process parameters that are investigated in this study are listed in Table 2.

Table 1 Properties of nitrogen used in analog computation

c_V / (J·(kg·K)$^{-1}$)	Thermal conductivity/ (W·(m·K)$^{-1}$)	Viscosity/ (kg·(m·s)$^{-1}$)	Molecular weight
1 040.67	0.024 2	1.663×10^{-5}	28.013 4

Table 2 Parameter of numerical model of gas flow field

Annular slit width D/mm	Protrusion length H/mm	Atomization gas pressure p/MPa
0.3, 0.6, 0.9, 1.2	4.5	4.5
1.2	4.5	1, 2, 3, 4, 5, 6, 7
1.2	2, 3, 4, 5, 6, 7, 8	4.5

2.4 Solving method

The implicit format in the coupling algorithm is adopted for the solver, which is then used to solve continuity, momentum, and energy equations. The second-order upwind scheme is used as a flux computing method. In the computing process, the flow Courant number is set as a reasonably stable value (1—3). The inlet boundary is taken for initialization operation, and the number of iterations is generally set as 20 000. The computation ends when the significant variables of flow field no longer change through the computation for a certain time and the difference value of the total inlet and outlet flow quantities in the computational domain is below the order of magnitude of 10^{-6} (the difference value is calculated between 20 iterations).

2.5 Grid independence study

A detailed study was carried out to prevent influences of grid size on results. Moreover, high-quality meshing with increasing fineness was performed to evaluate influences on results. The numerical simulation conditions are listed in Table 3. Three grids of increasing fineness were used in the work (grid 1: 2 500 000 elements; grid 2: 5 000 000 elements; and grid 3: 10 000 000 elements). To determine the influence of grid refinement on the CFD solution and to ensure grid independence, the axial gas velocity v_y and pressure were monitored along the lines AB and CD (Fig.2), respectively, before the numerical simulation. The axial gas velocity v_y and pressure variations along these two lines for each different grid are shown in Figs. 3, 4, and give the Richardson extrapolation result as a reference. The numerical simulation results of error analysis based on the three numerical grids are given in Table 4. In Table 4, k is the numerical grid, p_t the melt delivery tube tip pressure, L_r the length of the recirculation zone, and GCI the grid convergence index[24]. It can be seen that the velocity and pressure field for grids 2 and 3 are grid independent[25-26]. Therefore, it is appropriate to use grid 2 in the numerical experiments.

Table 3 Numerical simulation conditions of gas flow field

Annular slit width D/mm	Protrusion length H/mm	Atomization gas pressure p/MPa
1.2	4.5	5

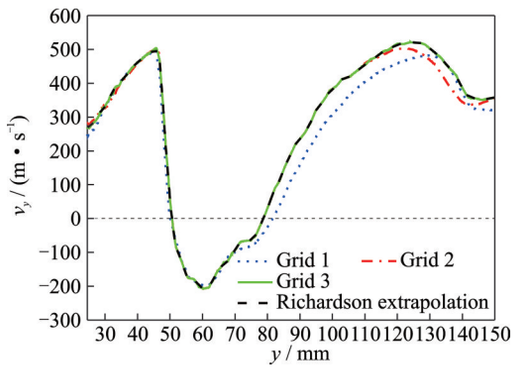

Fig.3 Influences of grid size on predicted axial gas velocity v_y along line AB ($x = z = 0$)

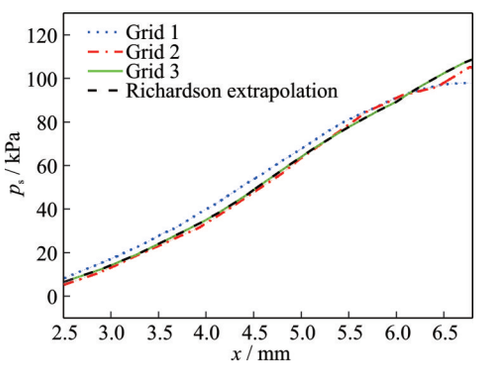

Fig.4 Influences of grid size on predicted static pressure distribution along line CD ($y = 24.5$ mm)

Table 4 Numerical simulation results of error analysis with different numerical grids

k	p_t / Pa	L_r / mm	$GCI_{k+1,k}$ (p_t)/%	$GCI_{k+1,k}$ (L_r)/%
1	1 604.446	31.556	4.545	3.382
2	1 109.978	28.325	1.538	0.456
3	958.139	28.252		

2.6 Validity verification of numerical calculation methodology

To verify validity of computing methodology, numerical simulation on the experimental research results of Shanghai Research Institute of Materials concerning the relationship between the atomization gas pressure and the front-end static pressure of the melt delivery tube was carried out. Computing conditions of different working conditions in the numerical calculation is listed in Table 5. Comparison between numerical simulation results in this study and experimental results is shown in Fig.5, finding that the numerical simulation value and the measured value of the front-end static pressure of the melt delivery tube have the same variation trend with atomization gas pressure (for the cases with $p \geqslant 3$ MPa, a certain discrepancy is observed between numerical results and experimental data, which may be caused by the turbulence model used in the simulation calculation). This demonstrates that the above numerical calculation methodology is feasible to simulate similar problems.

Table 5 Numerical simulation conditions of gas flow field under different atomization gas pressures

Annular slit width D/mm	Protrusion length H/mm	Atomization gas pressure p/MPa
1.2	4.5	1, 2, 3, 3.5, 4, 4.5

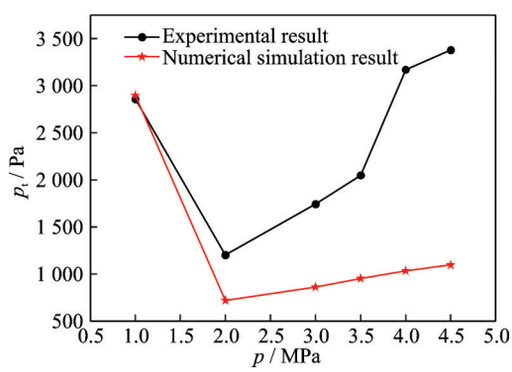

Fig.5 Comparison of static pressure at front end of melt delivery tube for numerical simulation and experiment

3 Results and Discussion

3.1 Basic features of gas flow field nearby atomizing nozzle outlet

Figs.6(a—c) show the velocity vector graph, streamline pattern and temperature cloud diagram of the gas flow field in the atomizing chamber under 5 MPa atomization gas pressure, 4.5 mm protrusion length, and 1.2 mm annular slit width. Fig.6(d) displays the experimental result, namely the solidification-induced clogging phenomenon of metal melt near the central hole outlet at the front end of the melt delivery tube. From the velocity vector graph on the x-y plane near the front end of the melt delivery tube and streamline pattern on an x-z plane, high-velocity gas is located within the x-z plane near the front end wall surface of the melt delivery tube. The gas is subjected to the joint actions of the cen-

tripetal pressure gradient, which occurs in a radial direction towards the direction of the y axis (this is primarily caused by the three-dimensional swirling flow effect) and entraining force of jet flow at the gas outlet of the loop slit of the atomizer on the outer wall surface at the front end of the melt delivery tube. One part of the high-velocity gas flows in a coaxial spiral way at an accelerated speed towards the gas outlet of loop slit, while the other part makes the same flow towards the central gas outlet at the front end of the melt delivery tube. The temperature of the high-velocity gas initially rises gradually and then declines gradually along the direction of the centripetal pressure gradient. Gas velocity at the boundary between the two gas flow branches moving in direction x is 0, and had the highest temperature. When the high-velocity gas flow is close to the central gas outlet at the front end of the melt delivery tube, the flow is along the positive direction of axis y. Under the joint action of aspirating pressure at the front end of the melt delivery tube, the gas flowing out from the central gas outlet at the front end of the delivery tube flows in a coaxial spiral at an accelerated speed along the positive direction of axis y, as shown in Fig.6(c). This result is basically identical to the experimental result, that is, water atomization, as shown in Fig.6(d).

The velocity vector graph and streamline pattern in Figs.6(a—c) indicate that in actual gas atomization process, the gas flowing out of the gas outlet of the loop slit and metal melt flowing from the central hole at the front end of the melt delivery tube into the atomizing chamber can be regarded as a coaxial jet flow. The gas that comes into contact with the metal melt flowing from the central hole at the front end of the melt delivery tube into the atomizing chamber flows in a coaxial spiral at an accelerated speed along the positive direction of axis y. Subsequently, the surface of the liquid column will make coaxial spiral flow due to the viscous force applied by the gas on the surface of the column. This result is identical to the experimental result, that is, solidification of metal melt at the front end of the melt delivery tube, as shown in Fig.6(e). Chen and Yin[11] reached a similar conclusion through experimental studies.

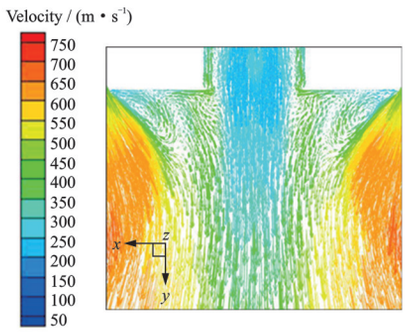

(a) Velocity vector graph on x-y plane nearby front end of melt delivery tube (the red line area in Fig.2) (1∶0.3)

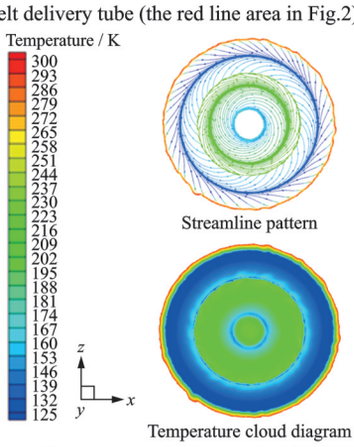

(b) Streamline pattern and temperature cloud diagram on x-z plane nearby front end ofmelt delivery tube (the white line area in Fig.2) (1∶0.54; y = 24.5 mm)

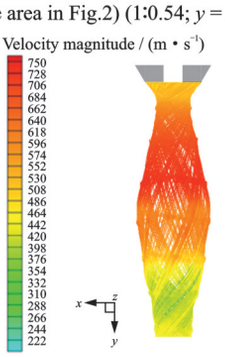

(c) Streamline pattern nearby outer wall surface at front end of melt delivery tube (the green line area in Fig.2) (1∶1.67)

(d) Water atomization photo(p = 1.5 MPa, H_2O)

(e) Photo of experimental result: Solidification of metal melt at front end of melt delivery tube (p = 4.5 MPa, 18Ni300)

Fig.6 Numerical simulation and experimental results

3.2 Effect of annular slit width on clogging phenomenon

Fig.7 shows the effect of the annular slit width D on radial change of static pressure at the front end of the melt delivery tube. The numerical simulation conditions are listed in Table 6.

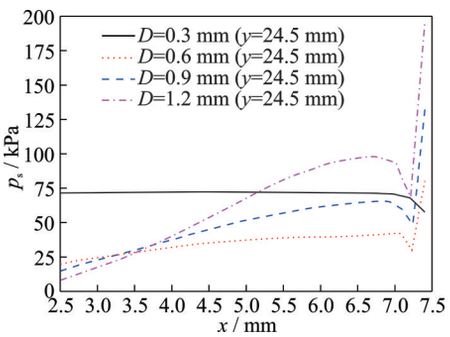

Fig.7 Radial change curve of static pressure at front end of melt delivery tube under different annular slit widths

Fig.7 shows that when pressure intensity in the working environment is 96 700 Pa, the aspirating pressure generated nearby the central gas outlet at the front end of the melt delivery tube gradually declines as the annular slit width increases. This pressure is always lower than environmental pressure intensity. At the time, working pressure intensity at the inlet is 4.5 MPa, and the smaller the aspirating pressure, the better the flow guidance. Hence, the atomizer had the best flow guiding effect when $D =$ 1.2 mm. Fig.7 further shows that static pressure intensity under radial distribution may not be a constant value. When 0.6 mm $\leqslant D \leqslant$ 1.2 mm, static pressure initially increases gradually, then rapidly decreases, and finally increases rapidly from near the central gas outlet at the front end of the melt delivery tube towards the outer wall surface. This effect is due to the supersonic gas flow ejected out of the gas outlet of the loop slit of the atomizer, which then expands and accelerates near the outer wall surface at the front end of the melt delivery tube. The expanded and accelerated supersonic gas flow will generate entrainment effect on the gas on the outer wall surface at the front end of the melt delivery tube and compress the gas at the front end of the delivery tube toward the central hole outlet direction at front end of the delivery tube. Then, static pressure near the front-end wall surface of the delivery tube initially increases gradually, then decreases rapidly and finally increases at a high speed along the radial direction. This effect is one of the reason why vibration primary breakup is generated at the central hole outlet at the front end of the delivery tube.

When $D = 0.3$ mm, the change in static pressure near the front-end wall surface of the melt delivery tube along the radial direction may be different from other nozzle types. Hence, the static pressure from near the central gas outlet at the front end of the delivery tube toward the outer wall surface at the front end of the delivery tube decreases. The supersonic gas flow ejected from gas outlet of loop slit of the atomizer weakens under-expansion degree near the outer wall surface at front end of the delivery tube due to reduction of mass flow rate. However, entrainment effect happens on the gas on the outer wall surface at the front end of the delivery tube. Therefore, the gas closer to the outer wall surface can be easily carried away by high-velocity gas flow flowing out of the gas outlet of the loop slit. Thus, pressure drop occurs at this position and is one of reasons for primary sheet breakup at front end of the melt delivery tube[27-29]. However, at the time, if aspirating pressure generated near the central gas outlet at front end of the melt delivery tube is at maximum, then the metal melt will slow down. More se-

Table 6 Numerical simulation conditions of gas flow field

Annular slit width D / mm	Inlet temperature T / K	Protrusion length H / mm	Atomization gas pressure p / MPa	Outlet pressure p_o / Pa	Outlet temperature T_o / K
0.3	300	4.5	4.5	96 700	300
0.6	300	4.5	4.5	96 700	300
0.9	300	4.5	4.5	96 700	300
1.2	300	4.5	4.5	96 700	300

riously, the gas will enter the crucible through the central hole at the front end of the melt delivery tube, thus causing melt blistering phenomenon. This phenomenon will even cause the solidification of metal melt and result in clogging.

In addition, Fig.7 further illustrates that the smaller the aspirating pressure at the front end of the melt delivery tube, the farther the position of boundary on the x-z plane is from the central hole outlet of the melt delivery tube and the greater the adverse pressure gradient toward the boundary. Because of the greater the distance from the central hole outlet at the front end of the melt delivery tube to the boundary, and the large adverse pressure gradient, the gas near the front-end wall surface of the delivery tube will arrive at the central hole outlet of the delivery tube at a higher velocity. As a result, under the joint action of aspirating pressure at the front end of the delivery tube, metal melt flowing from the central hole at the front end of the delivery tube into the atomizing chamber will more easily move as coaxial spiral flow at an accelerated speed along the positive direction of axis y in the gas atomizing process of metal melt, as shown in Figs.8—10.

According to the energy conservation equation, increasing gas velocity will surely result in temperature decline, as shown in Fig.11. In addition, Fig.11 shows that the smaller the aspirating pressure at the front end of the delivery tube, the greater the radial adverse pressure gradient, the lower the static temperature at the central hole outlet at the front end of the delivery tube. Therefore, in the actual gas atomization, the metal melt flowing from the central hole at the front end of the delivery tube into the atomiz-

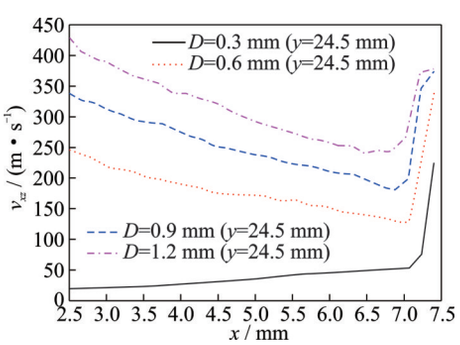

Fig.8 Radial change curve of v_{xz} at front end of melt delivery tube under different annular slit widths

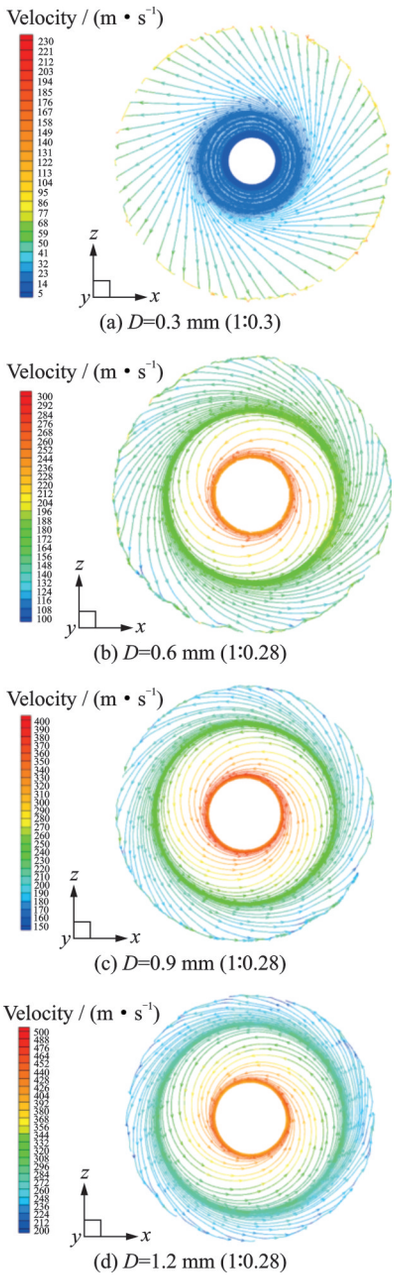

Fig.9 Streamline pattern on x-z plane at front end of melt delivery tube under different annular slit widths (y = 24.5 mm)

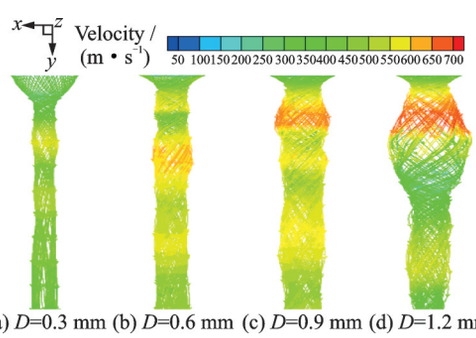

Fig.10 Streamline pattern nearby outer wall surface at front end of melt delivery tube under different annular slit widths (1∶0.78)

ing chamber can be more easily solidified, thus causing the clogging phenomenon, and powder production by atomization becomes impossible[11].

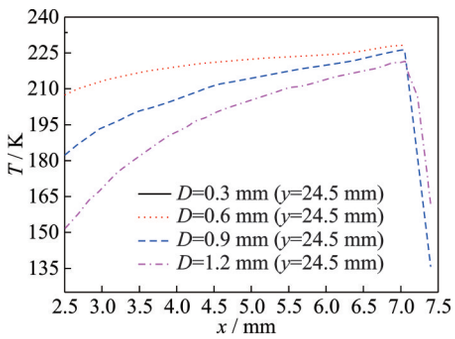

Fig.11 Radial change curve of static temperature at front end of melt delivery tube under different annular slit widths

Therefore, to prevent the metal melt from going through the clogging phenomenon due to solidification, the annular slit width should be reduced as far as possible on the precondition that aspirating pressure presents negative pressure on the nozzle atomization process ($0.3\ \text{mm} \leqslant D \leqslant 1.2\ \text{mm}$).

3.3 Effect of atomization gas pressure on clogging phenomenon

Fig.12 shows the effect of atomization gas pressure on the radial distribution of front-end static pressure of the melt delivery tube under protrusion length $H = 4.5$ mm of melt delivery tube and annular slit width $D = 1.2$ mm, numerical simulation conditions are listed in Table 7.

Fig.12 further shows that the radial distribution of front-end static pressure of the melt delivery tube may not be a uniform value. The pressure firstly increases, then decreases, and rapidly increases from

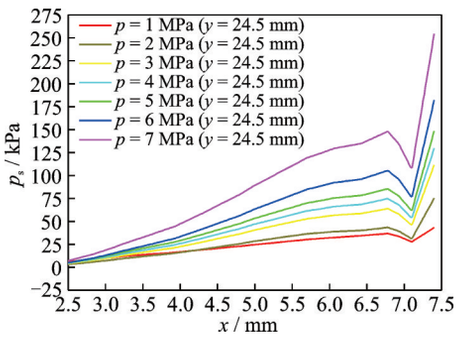

Fig.12 Radial change curve of front-end static pressure of melt delivery tube under different atomization gas pressures

the nearby central gas outlet at the front end of the melt delivery tube towards the outer wall surface. This effect occurs mainly because the supersonic gas flow, which is ejected out of the gas outlet of the loop slit of the atomizer, expands and accelerates near the outer wall surface at the front end of the delivery tube. The expanded and accelerated supersonic gas flow will generate entrainment effect on the gas on the outer wall surface at the front end of the delivery tube and compress the front-end gas of the melt delivery tube toward the central hole outlet at the front end of the delivery tube. Therefore, static pressure near the front-end wall surface of the delivery tube first increases, then decreases, and rapidly increases along the radial direction.

In Fig.12, as the atomization gas pressure increases, to enable the static pressure of atomization gas flow ejected out of gas outlet of loop slit of the atomizer to reach an equilibrium state with pressure intensity in the atomizing chamber, the under-expansion degree of high-velocity gas flow ejected out of gas outlet of loop slit near the outer wall surface at front end of the delivery tube is gradually enhanced.

Table 7 Numerical simulation conditions of gas flow field

Annular slit width D / mm	Inlet temperature T / K	Protrusion length H / mm	Atomization gas pressure p / MPa	Outlet pressure p_o / Pa	Outlet temperature T_o / K
1.2	300	4.5	1	96 700	300
1.2	300	4.5	2	96 700	300
1.2	300	4.5	3	96 700	300
1.2	300	4.5	4	96 700	300
1.2	300	4.5	5	96 700	300
1.2	300	4.5	6	96 700	300
1.2	300	4.5	7	96 700	300

Consequently, the entrainment effect on the gas on the front-end outer wall surface of the delivery tube and the compression degree of the front-end gas of the delivery tube toward the central hole outlet at the front end of the delivery tube are gradually enhanced. The change degree of static pressure near the front-end wall surface of the melt delivery tube along the radial direction in various phases is gradually elevated. The greater the adverse pressure gradient from the central hole outlet front-end of the melt delivery tube to the boundary, the higher the speed at which the gas near the boundary will arrive at the central hole outlet of the delivery tube in an accelerated way, but the increased amplitude will gradually reduce. When atomization gas pressure is 6 and 7 MPa, gas velocity within x-z plane near the front-end wall surface of the delivery tube is approximate. Hence, within a certain scope of atomization gas pressure, increasing the atomization gas pressure can elevate the gas velocity near the front-end wall surface of the delivery tube, which in turn will elevate the flow velocity of metal melt into the atomizing chamber through the central hole at the front end of the delivery tube, which allows the atomizing process to stabilize. However, after this scope is exceeded, continuing to enlarge the atomization gas pressure has a minor effect on gas velocity near the front-end wall surface of the delivery tube, as shown in Fig.13. This effect is one of the reason for the primary vibration breakup of the liquid column generated at the central hole outlet at the front end of the delivery tube.

Fig.14 shows the effect of atomization gas pressure on aspirating pressure at the front end of the delivery tube, where $\Delta p = p_t - p_o$, p_t represents the pressure value at the front end of the melt delivery tube, and p_o denotes the pressure intensity in the working environment. Fig.14 shows that when atomization gas pressure satisfies 1 MPa $\leqslant p \leqslant$ 2 MPa, aspirating pressure at the front end of the delivery tube is rapidly reduced with increasing atomization gas pressure, when 2 MPa $< p \leqslant$ 7 MPa, the fluctuation of aspirating pressure at the front end of the delivery tube is gradually enlarged as atomization gas pressure increases, which is primarily caused by different stagnation pressures on the central axis of the flow field (Fig.15)[17]. Large aspirating pressure will generate a slight aspirating action on metal melt such that the speed slows down for metal melt to flow into the atomizing chamber through the central hole at the front end of the delivery tube. The gas-melt ratio in mass flow rate is enlarged and the atomizing effect is improved.

Fig.16 displays the effect of atomization gas pressure on the radial distribution of the front-end static temperature of the delivery tube. Fig.16 fur-

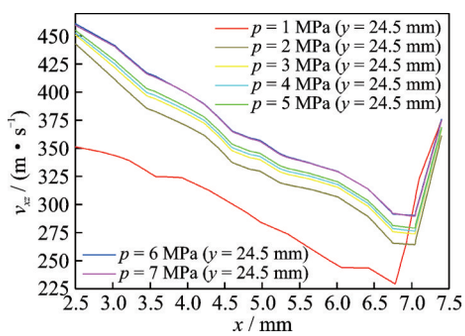

Fig.13 Radial change curve of front-end v_{xz} of melt delivery tube under different atomization gas pressures

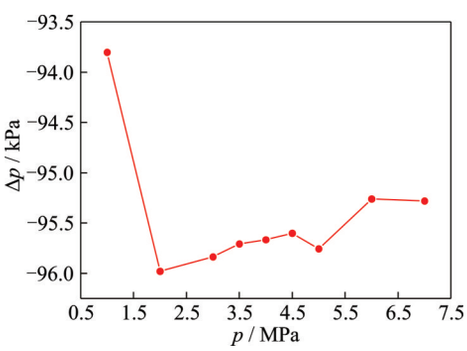

Fig.14 Effect of atomization gas pressure on aspiration pressure at front end of melt delivery tube

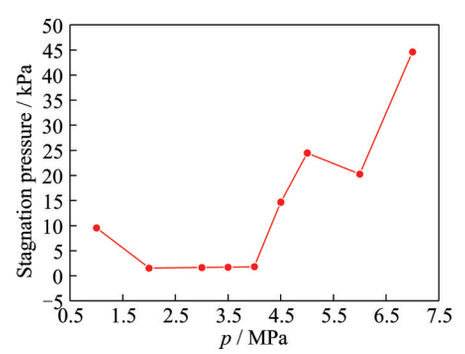

Fig.15 Effect of atomization gas pressure on stagnation pressure on central axis of flow field

ther shows that the radial distribution of static temperature at the front end of the delivery tube may not be a constant value. Instead, the temperature first rises to reach a maximum value and then rapidly declines from the nearby central gas outlet at the front end of the delivery tube toward the outer wall surface. This effect is mainly due to the behavior of gas velocity within the x-z plane at the front end of the delivery tube. First, gas velocity declines to reach minimum value and then rapidly rises from the nearby central gas outlet at the front end of the delivery tube toward the outer wall surface. From energy conservation law, increasing gas velocity will certainly lead to temperature drop, and thus, the static temperature near the front-end wall surface of the delivery tube presents an initial gradual rising and then rapidly declining variation trend along the radial direction.

Fig.16 further shows that as the atomization gas pressure increases, the static temperature near the front-end wall surface of the delivery tube gradually declines, but the decreased amplitude is gradually lowered. When atomization gas pressure is 6 and 7 MPa, the static temperature of the gas near the front-end wall surface of the delivery tube is approximate. This effect indicates that within a certain scope of atomization gas pressure, enlarging atomization gas pressure can reduce the static temperature of the gas near the front-end wall surface of the delivery tube. However, after this scope is exceeded, continuing to enlarge atomization gas pressure will have a minor effect on the static temperature of the gas near the front-end wall surface of the delivery tube (Fig.17). This effect is basically identical with the change of gas velocity within the x-z plane near the front end of the delivery tube with atomization gas pressure.

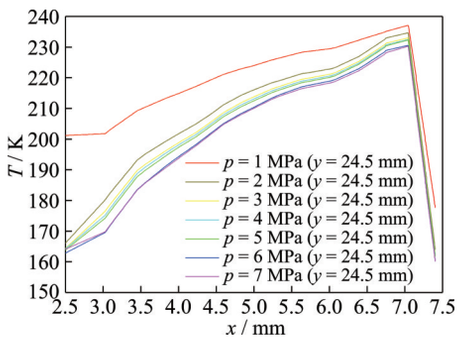

Fig.16 Radial change curve of front-end static temperature of the melt delivery tube under different atomization gas pressures

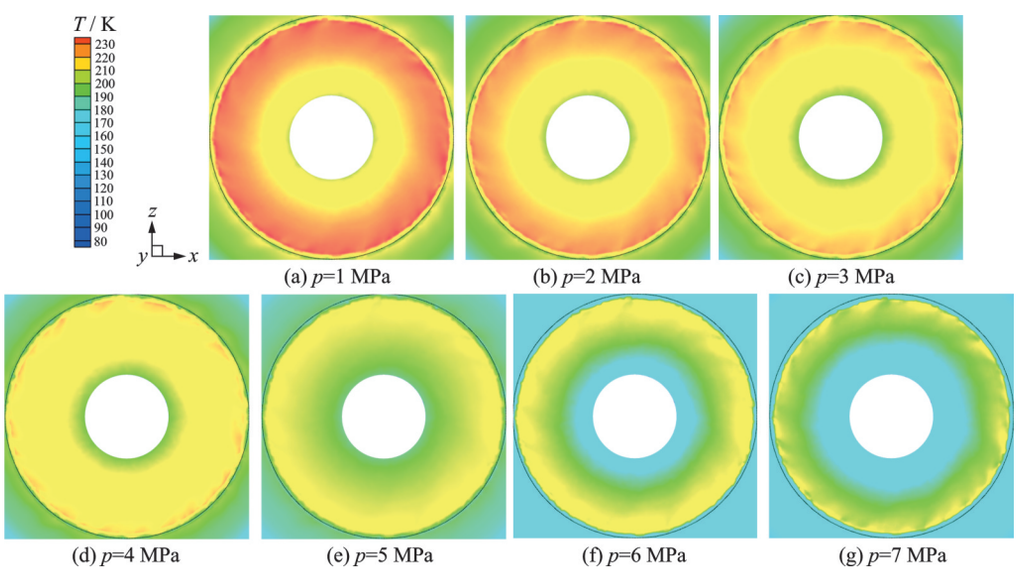

Fig.17 Temperature cloud diagram on x-z plane nearby front end of melt delivery tube under different atomization gas pressures (1 : 2.36)

Therefore, solidification of the metal melt flowing from the central hole at the front end of the delivery tube into the atomizing chamber causes the clogging phenomenon. Hence, atomization gas pressure should be reduced as far as possible on the precondition that effective atomization of the metal

melt is guaranteed in the atomizing process of the nozzle ($4\ \text{MPa} < p \leqslant 7\ \text{MPa}$)[17].

3.4 Effect of protrusion length of melt delivery tube on clogging phenomenon

Fig.18 shows the change curves of front-end static pressure of the melt delivery tube along the radial direction under different protrusion lengths of the melt delivery tube under $D = 1.2$ mm and $p = 4.5$ MPa. Fig.19 displays the change of front-end aspirating pressure of the melt delivery tube with its protrusion length, numerical simulation conditions are listed in Table 8.

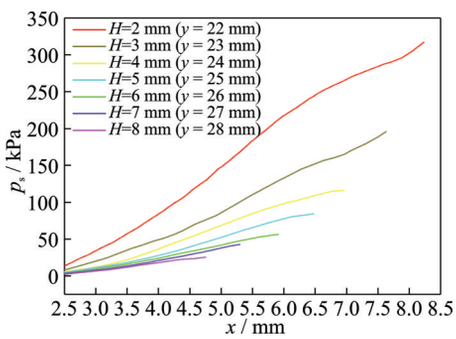

Fig.18 Radial change curves of front-end static pressure of melt delivery tube under different protrusion lengths of melt delivery tube

Further, Fig.18 indicates that static pressure, which is distributed along the radial direction at the front end of the delivery tube, may not be a constant, but instead, has an adverse pressure gradient. The static pressure then declines as the protrusion length of the delivery tube increases. Supersonic gas flow ejected out of the gas outlet of the loop slit of the atomizer goes through expansion and acceleration near the outer wall surface at the front end of the delivery tube. The expanded and accelerated supersonic gas flow around the front end of the delivery tube will compress the gas at the front end of the delivery tube toward the central gas outlet at the front end of the delivery tube. As a result, static pressure near the wall surface at the front end of the delivery tube is gradually elevated along the radial direction.

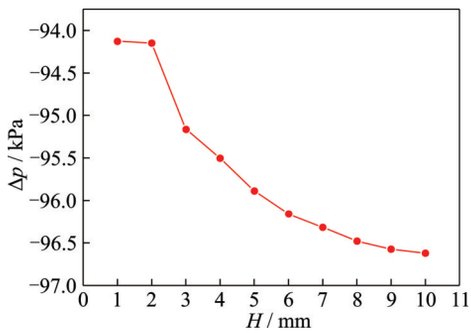

Fig.19 Effect of protrusion length of melt delivery tube on aspiration pressure at front end of melt delivery tube

Moreover, Fig.18 shows that as the protrusion length of the delivery tube increases, the supersonic gas flow ejected out of the gas outlet of the loop slit of the atomizer gradually flows along the outer wall surface of the protruding part of the delivery tube due to Coanda effect. The supersonic gas flow, which originally undergoes through expansion and acceleration, is gradually expanded and accelerated only outside the outer wall surface of the protrusion length of the melt delivery tube. The gas flow will recover by expanding around only when the supersonic gas flow reaches the outer wall surface at the front end of the delivery tube. At that time, as the supersonic gas flow goes through expansion and ac-

Table 8 Numerical simulation conditions of gas flow field

Annular slit width D / mm	Inlet temperature T / K	Protrusion length H / mm	Atomization gas pressure p / MPa	Outlet pressure p_o / Pa	Outlet temperature T_o / K
1.2	300	2	4.5	96 700	300
1.2	300	3	4.5	96 700	300
1.2	300	4	4.5	96 700	300
1.2	300	5	4.5	96 700	300
1.2	300	6	4.5	96 700	300
1.2	300	7	4.5	96 700	300
1.2	300	8	4.5	96 700	300

celeration for a certain distance, static pressure is already somehow decreased. The under-expansion degree of the supersonic gas flow near the outer wall surface at the front end of the delivery tube is gradually weakened. Moreover, the compression degree of the gas near the front end of the delivery tube is gradually lowered. Consequently, the adverse pressure gradient of the static pressure near the wall surface at the front end of the delivery tube along the radial direction is gradually reduced. Furthermore, the adverse pressure gradient at the front end of the delivery tube along the radial direction is gradually reduced as the protrusion length of the delivery tube increases. However, as the supersonic gas flow arriving near the outer wall surface at the front end of the delivery tube has gone through expansion and acceleration for a certain distance, its gas flow velocity is gradually elevated. The speed at which the gas within the x-z plane at the front end of the delivery tube arrives near the central hole outlet of the delivery tube in an accelerated way under different protrusion lengths of the melt delivery tube is approximate. Hence, enlarging the protrusion length of the delivery tube has a minor effect on the speed at which the metal melt flows into the atomizing chamber through the central hole at the front end of the delivery tube, as shown in Figs. 20 and 21. Fig. 22 shows the effect of protrusion length of the melt delivery tube on the radial distribution of the front-end static temperature of the delivery tube.

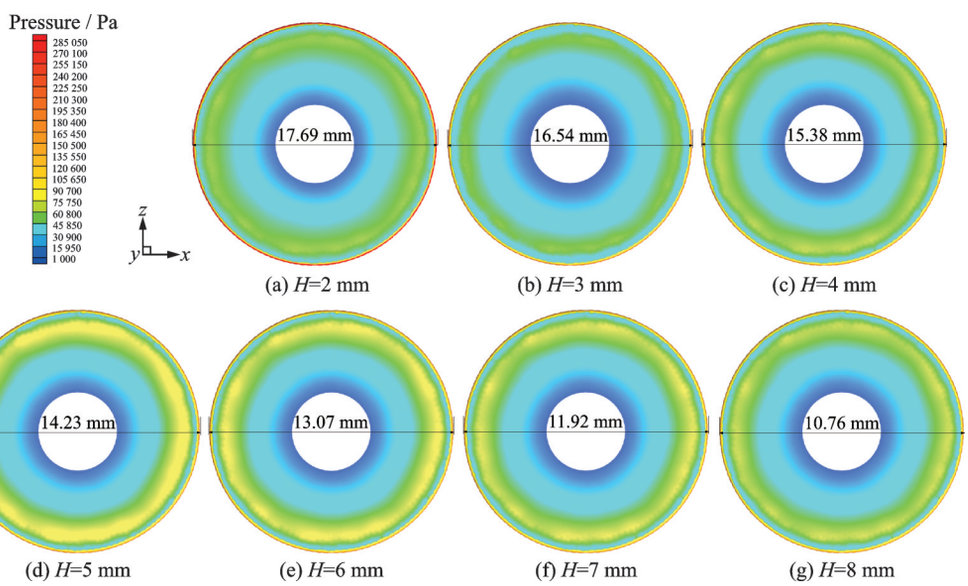

Fig.20 Static gas pressure distribution on x-z plane nearby front end of melt delivery tube under different protrusion lengths of melt delivery tube

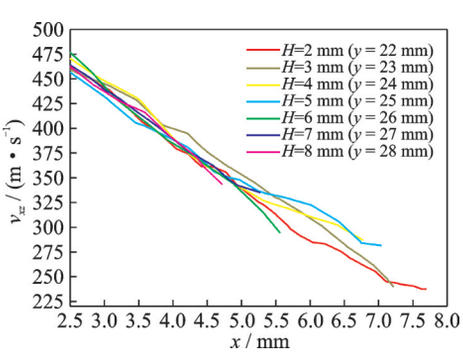

Fig.21 Effect of protrusion length of melt delivery tube on radial distribution of front-end v_{xz} of melt delivery tube

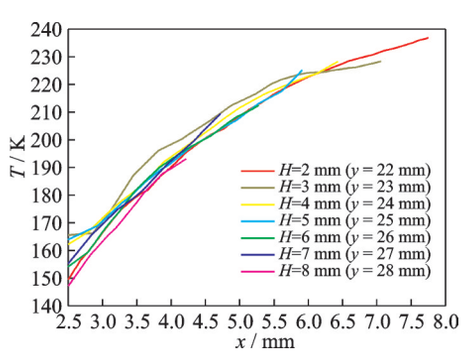

Fig.22 Effect of protrusion length of melt delivery tube on radial distribution of front-end static temperature of melt delivery tube

Fig.22 further shows that the radial distribution of the front-end static temperature of the melt delivery tube may not be a constant value. Instead, the temperature gradually rises from near the central gas outlet at the front end of the delivery tube toward the outer wall surface. The gas flow velocity within the x-z plane at the front end of the delivery tube gradually decreases from near the central gas outlet at the front end of the delivery tube toward the outer wall surface. According to energy conservation law, the reduction of gas velocity will lead to temperature rise. Static temperature near the front-end wall surface of the delivery tube gradually rises along the radial direction. As the protrusion length of the delivery tube increases, the radial distribution of the front-end static temperature of the delivery tube is not obviously different. This value is identical to the change of gas velocity within the x-z plane near the front end of the delivery tube with the protrusion length of the delivery tube.

In addition, Fig.22 shows that as the protrusion length of the delivery tube increases, the static temperature near the central hole outlet at the front end of the delivery tube changes little. The static temperature near the central hole outlet at the front end of the melt delivery tube will slowly decline as the protrusion length of the delivery tube increases, but only when the protrusion length of the delivery tube exceeds a certain value ($H \geqslant 4$ mm).

Fig.19 indicates that the greater the protrusion length of the delivery tube, the smaller the adverse pressure gradient of static pressure near the front-end wall surface of the delivery tube along the radial direction, as well as smaller aspirating pressure at the front end of the delivery tube. The small aspirating pressure will generate a great aspirating effect on the metal melt such that the metal melt in the delivery tube smoothly flows downward, which is conducive to the stability of the atomizing process.

Therefore, the effect of the protrusion length of the delivery tube on the radial distribution of front-end static temperature in the delivery tube is minor. However, to prevent as far as possible metal melt from the clogging phenomenon caused by solidification, the protrusion length of the delivery tube should be reduced as far as possible on the precondition that aspirating pressure presents negative pressure in the nozzle atomization process (1 mm $\leqslant H \leqslant$ 10 mm).

4 Conclusions

(1) Fluent software was used to simulate the single-phase gas flow field of the close-coupled supersonic vortical loop slit atomizer under different structural parameters of the nozzle and operating parameters. Annular slit width D of the atomizer and pressure p of the atomization gas had significant effects on aspirating pressure at the front end of the delivery tube and static temperature near the central hole outlet at front end of the delivery tube. When atomization gas pressure is $p = 4.5$ MPa, the greater the annular slit width D, the lower the static temperature near the central hole outlet at front end of the delivery tube, and the smaller the front-end aspirating pressure of the delivery tube. The small aspirating pressure could help the metal melt to flow downward smoothly to prevent effectively the reduction of static temperature of the gas near the central hole outlet at the front end of the delivery tube and solidification of the metal melt, which would cause clogging phenomenon.

(2) Atomization gas pressure becomes greater under $D = 1.2$ mm and 1 MPa $\leqslant p \leqslant$ 2 MPa. Aspirating pressure at the front end of the delivery tube is rapidly decreased. This effect can prevent the metal melt from clogging phenomenon. When 2 MPa $< p \leqslant$ 7 MPa, the greater the atomization gas pressure, the lower the static temperature near the central hole outlet at the front end of the delivery tube, the greater the aspirating pressure at front end of the delivery tube. Large aspirating pressure could reduce the velocity at which the metal melt flows into the atomizing chamber through the central hole at the front end of the delivery tube. As a result, the effect of preventing the metal melt from clogging phenomenon caused by solidification is restricted.

(3) Under $p = 4.5$ MPa and $D = 1.2$ mm conditions, the greater the protrusion length H of the delivery tube, the smaller the aspirating pressure at the front end of the delivery tube. However, the

static temperature near the central hole outlet at the front end of the delivery tube was approximate to prevent effectively the occurrence of clogging phenomenon of metal melt. However, due to small aspirating pressure, the velocity at which the metal melt flowed into the atomizing chamber through the central hole at the front end of the delivery tube was elevated, and gas-melt ratio in mass flow rate was reduced. This effect was adverse to the improvement of the atomizing performance.

References

[1] OUYANG H W, CHEN X, YU W T, et al. Progress and prospect on the gas atomization[J]. Powder Metallurgy Technology, 2007, 25(1): 53-63.

[2] ZHANG M, XU G. Aluminum powder production through preheated compressed air spraying[J]. Light Alloy Fabrication Technology, 1990, 18(8): 36-48.

[3] HAN F L, GE C D. Steel powder production[M]. 1st ed. Beijing: Metallurgical Industry Press, 1980.

[4] ANDERSON I E, FIGLIOLA R S, MORTON H. Flow mechanisms in high-pressure gas atomization [J]. Materials Science & Engineering A, 1991, 148 (1): 101-114.

[5] MI J, FIGLIOLA R S, ANDERSON I E. A numerical simulation of gas flow field effects on high pressure gas atomization due to operating pressure variation [J]. Materials Science & Engineering A, 1996, 208 (1): 20-29.

[6] MI J, FIGLIOLA R S, ANDERSON I E. A numerical investigation of gas flow effects on high-pressure gas atomization due to melt tip geometry variation[J]. Metallurgical & Materials Transactions B, 1997, 28 (5): 935-941.

[7] CUI C S, CAO F Y, LI Q C. Formation mechanism of the pressure zone at the tip of the melt delivery tube during the spray forming process[J]. Journal of Materials Processing Technology, 2003, 137(1): 5-9.

[8] MATES S P, SETTLES G S. A study of liquid metal atomization using close-coupled nozzles, Part 1: Gas dynamic behavior[J]. Atomization and Sprays, 2005, 15(1): 19-40.

[9] ZEOLI N, GU S. Computational simulation of metal droplet break-up, cooling and solidification during gas atomization[J]. Computational Materials Science, 2008, 43(2): 268-278.

[10] LI X G, FRITSCHING U. Process modeling pressure-swirl-gas-atomization for metal powder production [J]. Journal of Materials Processing Technology, 2017, 239(1): 1-17.

[11] CHEN S Z, YIN Z M. Effect of vortical nozzle on leakage pipe extension[J]. Material Science and Technology, 1998, 6(1): 69-72.

[12] LIU F P. Analysis on design parameters of the vortical loop slit atomizer[J]. Powder Metallurgy Technology, 2011, 29(5): 339-343.

[13] MA Y F, ZHANG Z M. Simulation and analysis of gas flow field in metallic solution atomizer[J]. International Journal of Fluid Dynamics, 2017, 5(2): 76-82.

[14] MOTAMAN S, MULLIS A M, COCHRANE R F, et al. Numerical and experimental modelling of back stream flow during close-coupled gas atomization [J]. Computers & Fluids, 2013, 88(1): 1-10.

[15] AYDIN O, UNAL R. Experimental and numerical modeling of the gas atomization nozzle for gas flow behavior[J]. Computers & Fluids, 2011, 42(1): 37-43.

[16] PRASHANTH W S, THOTARATH S L, SARKAR S, et al. Experimental investigation on the effect of melt delivery tube position on liquid metal atomization[J]. Advanced Powder Technology, 2021, 32(3): 693-701.

[17] ZHANG M, ZHANG Z M, ZHANG Y Q, et al. CFD-based numerical simulation of gas flow field characteristics in close-coupled vortical loop slit gas atomization[J]. Atomization and Sprays, 2021, 31(7): 17-47.

[18] MALY M, SAPIK M, CEJPEK O, et al. Effect of spill orifice geometry on spray and control characteristics of spill-return pressure-swirl atomizers[J]. Experimental Thermal and Fluid Science, 2019, 106(9): 159-170.

[19] FAN X J, LIU C X, MU Y, et al. Experimental investigations of spray characteristics of a pressure-swirl atomizer[J]. Proceedings of the Institution of Mechanical Engineers Part A—Journal of Power and Energy, 2020, 234(5): 643-654.

[20] OCHOWIAK M. Discharge coefficient of effervescent atomizers with the swirl motion phenomenon[J]. Experimental Thermal and Fluid Science, 2016, 79 (12): 44-51.

[21] RAZEGHI A, ERTUNC O. Numerical investigation of multiphase flow inside a pressure swirl atomizer at the initial stage of injection[J]. Atomization and Sprays, 2018, 28(5): 417-441.

[22] WANG P, LI J, WANG X, et al. Impact mechanism of gas temperature in metal powder production via gas atomization[J]. Chinese Physics B, 2021, 30(5): 1-15.

[23] MENTER F R. Two-equation eddy-viscosity turbulence models for engineering applications[J]. AIAA Journal, 1994, 32(8): 1598-1605.

[24] ROACHE P J. Perspective: A method for uniform reporting of grid refinement studies[J]. Journal of Fluids Engineering, 1994, 116(3): 405-413.

[25] CELIK I B, GHIA U, ROACHE P J, et al. Procedure for estimation and reporting of uncertainly due to

discretization in CFD applications[J]. Journal of Fluids Engineering, 2008, 130(7): 1-4.
[26] KARIMI M, AKDOGAN G, DELLIMORE K H, et al. Quantification of numerical uncertainly in computational fluid dynamics modelling of hydrocyclones [J]. Computers & Chemical Engineering, 2012, 43 (33): 45-54.
[27] SRIVASTAVA V C, OJHA S N. Effect of aspiration and gas-melt configuration in close coupled nozzle on powder productivity[J]. Powder Metallurgy, 2006, 49(3): 213-218.
[28] TING J, PERETTI M W, EISEN W B. The effect of wake-closure phenomenon on gas atomization performance[J]. Materials Science & Engineering A, 2002, 326(1): 110-121.
[29] OUYANG H W, HUANG B Y, CHEN X, et al. Melt metal sheet breaking mechanism of close-coupled gas atomization[J]. Transactions of Nonferrous Metals Society of China, 2005, 15(5): 985-992.

Acknowledgements This work was supported by the Priority Academic Program Development of Jiangsu Higher Education Institutions (PAPD) and the Simulation and Test of the Flow Field of Gas Atomization Nozzle (No. 1001-KFA19184).

Authors Mr. **ZHANG Min** received his M.S. degree from Kunming University of Science and Technology in 2016. He is currently a Ph.D. candidate at College of Aerospace Engineering, Nanjing University of Aeronautics and Astronautics (NUAA). His research interests include experimental fluid mechanics and metal melt gas atomization.

Prof. **ZHANG Zhaoming** received his B.S. and M.S. degrees from NUAA in 1984 and 1987, respectively. He is currently a professor at College of Aerospace Engineering, NUAA. His research interests include aircraft test technology and wind tunnel test technique.

Author contributions Prof. **ZHANG Zhaoming** contributed to the background of the study, designed the study and prepared the manuscript. Mr. **ZHANG Min** contributed to the discussion and simulation analysis as well as all the drafts. Mr. **ZHANG Yanqi**, Mr. **LU Yuanjing** and Dr. **LU Lin** contributed to the discussion and the background of this study. Prof. **ZHANG Zhaoming** reviewed the manuscript. All authors commented on the manuscript draft and approved the submission.

Competing interests The authors declare no competing interests.

(Production Editor: SUN Jing)

旋涡环缝式雾化器气体流场对堵嘴现象的影响

章 敏[1], 张召明[1], 张彦奇[1], 卢远靖[1], 卢 林[2]
(1.南京航空航天大学航空学院,南京 210016,中国; 2.上海材料研究所,上海 200437,中国)

摘要:为研究旋涡环缝式雾化器喷嘴出口附近雾化室内气体流场基本特征及其对堵嘴现象的影响机理,在不同的环缝宽度、雾化气体压强和导液管突出长度条件下,采用计算流体动力学软件Fluent对旋涡环缝式雾化器喷嘴出口附近雾化室内气流场进行数值模拟。结果表明,雾化气体压强$p=4.5$ MPa时,环缝宽度D越大,导液管前端中心孔出口附近的静温越低,导液管前端抽吸压强越小,能有效防止金属溶体堵嘴现象的发生。在环缝宽度$D=1.2$ mm条件下,当雾化气体压强1 MPa$\leqslant p\leqslant$2 MPa时,雾化气体压强越大,导液管前端抽吸压强迅速减小,有利于防止金属溶液发生堵嘴现象,而当雾化气体压强$p>2$ MPa时,雾化气体压强越大,导液管前端中心孔出口附近的静温越低,导液管前端抽吸压强越大,从而防止金属溶体因凝固而发生堵嘴现象的效果有限。在雾化气体压强$p=4.5$ MPa,环缝宽度$D=1.2$ mm的条件下,导液管突出长度H越大,导液管前端抽吸压强越小,而导液管前端中心孔出口附近的静温却很接近,从而可有效防止金属溶体堵嘴现象的发生,但小的抽吸压强使得金属熔体通过导液管前端中心孔流入雾化室的速度增大,气液质量流率比减小,不利于雾化性能的提高。

关键词:旋涡环缝式雾化器;环缝宽度;雾化气体压强;导液管突出长度;气体流场;数值模拟